

Rational molecular engineering towards efficient heterojunction solar cells based on organic molecular acceptors

Kaiyan Zhang(张凯彦), Peng Song(宋朋), Fengcai Ma(马凤才), and Yuanzuo Li(李源作),

Citation: Chin. Phys. B, 2024, 33 (**6**): 068402. DOI: 10.1088/1674-1056/ad2a6a
Journal homepage: http://cpb.iphy.ac.cn; http://iopscience.iop.org/cpb

What follows is a list of articles you may be interested in

An artificial neural network potential for uranium metal at low pressures

Maosheng Hao(郝茂生) and Pengfei Guan(管鹏飞)
Chin. Phys. B, 2023, 32 (**9**): 098401. DOI: 10.1088/1674-1056/acd8a4

Applications and functions of rare-earth ions in perovskite solar cells

Limin Cang(苍利民), Zongyao Qian(钱宗耀), Jinpei Wang(王金培), Libao Chen(陈利豹), Zhigang Wan(万志刚), Ke Yang(杨柯), Hui Zhang(张辉), and Yonghua Chen(陈永华)
Chin. Phys. B, 2022, 31 (**3**): 038402. DOI: 10.1088/1674-1056/ac373a

Theoretical investigation of halide perovskites for solar cell and optoelectronic applications

Jingxiu Yang(杨竞秀), Peng Zhang(张鹏), Jianping Wang(王建平), and Su-Huai Wei(魏苏淮)†
Chin. Phys. B, 2020, 29 (**10**): 108401. DOI: 10.1088/1674-1056/abb3f6

SiO_2 nanoparticle-regulated crystallization of lead halide perovskite and improved efficiency of carbon-electrode-based low-temperature planar perovskite solar cells

Zerong Liang(梁泽荣), Bingchu Yang(杨兵初), Anyi Mei(梅安意), Siyuan Lin(林思远), Hongwei Han(韩宏伟), Yongbo Yuan(袁永波), Haipeng Xie(谢海鹏), Yongli Gao(高永立), Conghua Zhou(周聪华)
Chin. Phys. B, 2020, 29 (**7**): 078401. DOI: 10.1088/1674-1056/ab8da5

Photocurrent improvement of an ultra-thin silicon solar cell using the localized surface plasmonic effect of clustering nanoparticles

F Sobhani, H Heidarzadeh, H Bahador
Chin. Phys. B, 2020, 29 (**6**): 068401. DOI: 10.1088/1674-1056/ab836d

---

Rational molecular engineering towards efficient heterojunction solar cells based on organic molecular acceptors

Kaiyan Zhang(张凯彦)[1,2], Peng Song(宋朋)[3,†], Fengcai Ma(马凤才)[3], and Yuanzuo Li(李源作)[1,2,‡]

[1] *College of Materials Science and Engineering, Northeast Forestry University, Harbin* 150040, *China*
[2] *College of Science, Northeast Forestry University, Harbin* 150040, *China*
[3] *Department of Physics, Liaoning University, Shenyang* 110036, *China*

(Received 30 October 2023; revised manuscript received 4 February 2024; accepted manuscript online 19 February 2024)

The selection of photoactive layer materials for organic solar cells (OSCs) is essential for the photoelectric conversion process. It is well known that chlorophyll is an abundant pigment in nature and is extremely valuable for photosynthesis. However, there is little research on how to improve the efficiency of chlorophyll-based OSCs by matching chlorophyll derivatives with excellent non-fullerene acceptors to form heterojunctions. Therefore in this study we utilize a chlorophyll derivative, Ce_6Me_3, as a donor material and investigate the performance of its heterojunction with acceptor materials. Through density functional theory, the photoelectric performances of acceptors, including the fullerene derivative $PC_{71}BM$ and the terminal halogenated non-fullerene DTBCIC series, are compared in detail. It is found that DTBCIC-Cl has better planarity, light absorption, electron affinity, charge reorganization energy and charge mobility than others. Ce_6Me_3 has good energy level matching and absorption spectral complementarity with the investigated acceptor molecules and also shows good electron donor properties. Furthermore, the designed Ce_6Me_3/DTBCIC interfaces have improved charge separation and reorganization rates (K_{CS}/K_{CR}) compared with the $Ce_6Me_3/PC_{71}BM$ interface. This research provides a theoretical basis for the design of photoactive layer materials for chlorophyll-based OSCs.

Keywords: organic solar cells, density functional theory, chlorophyll derivative, non-fullerene acceptors

PACS: 84.60.Jt, 88.40.jr, 88.40.hj **DOI:** 10.1088/1674-1056/ad2a6a

1. Introduction

With the rapid development of society, the problems associated with the excessive consumption of fossil fuels and energy shortages have become increasingly prominent; more attention is therefore being devoted to the exploitation and utilization of renewable clean energy, such as solar energy. Organic solar cells (OSCs), which convert light into electrical energy, have attracted the attention of a wide range of researchers owing to their potential strengths, including low price, ease of manufacture and light weight.[1–6] Generally, OSC devices consist of cathodes, anodes and heterojunction active layers comprising donor and acceptor materials.[7–9] The crucial part is the active layer, which affects the optoelectronic performance of OSCs.[10–12] The working mechanism can be summarized as follows.[13,14] When the active layer is illuminated, the excited electrons are conveyed from the highest occupied molecular orbital (HOMO) of the donor to its lowest unoccupied molecular orbital (LUMO). Electrons are then transmitted from the donor's LUMO to the acceptor's LUMO when the LUMO level of the donor is higher than that of the acceptor. Next, electrons are transported in the acceptor material and collected at the cell's cathode. The holes are transported through the donor material and transferred to the anode.

Significant research has been carried out on OSC donor materials. In earlier work, Heeger *et al.*[15] blended polymer materials as the donor with $PC_{61}BM$ and spin-coated the film as the active layer. Salima *et al.*[16] later optimized the device and improved its photoelectric conversion efficiency (PCE) to reach 2.9%. Nguyen *et al.*[17] investigated the influence of alkyl side chain size on phase separation in P3HT/$PC_{61}BM$ hybrid films and found that P3HT had the highest PCE of 2.55%. Since chlorophyll and its derivatives are abundant in nature and have good electronic excitation energy and environmentally friendly functionality, more and more researchers have been studying them as solar cell donor materials. For example, Wang *et al.*[18] found that chlorophyll as the donor and fullerenes and their derivatives as electron acceptors in chlorophyll-based OSCs could increase the exciton dissociation at the donor/acceptor (D/A) interface. Duan *et al.*[19] used a chlorophyll derivative and the fullerene derivative $PC_{71}BM$ as donor and acceptor of the active layer, respectively, to fabricate an OSC and achieved a high PCE. Later, Duan *et al.*[20] also found that for dye-sensitized solar cells, synthesizing chlorophyll with carboxylic acid moieties as binding sites with semiconductors can improve the effectiveness of dye-sensitized solar cells. For OSCs, chlorophyll without carboxyl substituent is more suitable as the donor material. For perovskite solar cells, self-assembled aggregates of chlorophyll derivatives have been proven to be appropriate as a hole trans-

†Corresponding author. E-mail: songpeng@lnu.edu.cn
‡Corresponding author. E-mail: yzli@nefu.edu.cn

© 2024 Chinese Physical Society and IOP Publishing Ltd

port layer. Recently, some works also prepared OSC devices with chlorophyll derivatives as donor materials by a continuous spin-coating method.[21] Although the PCE of these devices is currently limited, their cheap price and the excellent characteristics of chlorophyll are very attractive and provide significant potential for the design of more efficient solar cells. Chlorophyll and its derivatives can also be easily synthesized by substituting different functional groups on the periphery of the tetrapyrrole ring to regulate the photochemical properties.

In addition, it is known from previous studies that acceptors of OSCs mainly depend on fullerene derivatives. The fullerenes and their derivatives have excellent electron mobility and charge transport as acceptor materials, but their absorption in the visible-light region is weak and the tunability of their energy level is limited.[22–24] Consequently, several meaningful works have concentrated on non-fullerene acceptors (NFAs) that can overcome these problems.[25–28] OSCs based on NFAs have been found to possess higher light-harvesting capabilities, tunable energy gaps and absorption spectra, which can achieve high PCEs.[29–31] So, it is important to find excellent NFA acceptors that can match chlorophyll derivatives to form heterojunctions to further enhance the improvement of chlorophyll-based OSCs. Among the NFAs with acceptor–donor–acceptor (A–D–A) structures, Y6 is the most extensively investigated as a small molecule acceptor (SMA). Yu *et al.*[32] discovered that this molecule has outstanding properties and is a good match with the donor molecule, achieving an efficiency of $> 16\%$. The A–D–C–D–A framework formed by decomposing the donor group in the A–D–A structure into D–C–D parts (C refers to a central core unit) helps to simplify the molecular synthesis process and has the potential to achieve enhanced optoelectronic properties.[33] Liu *et al.*[34] introduced BTzO-4F into an A–D–C–D–A structured acceptor molecule as an intermediate core unit to construct an OSC with a high efficiency of 14%.

In this work, we theoretically study the performance of the donor Ce_6Me_3 (a photosensitizer chlorin e6 that can be easily synthesized from the chlorophyll *a* molecule), the fullerene acceptor $PC_{71}BM$, A–D–C–D–A-structured NFAs and donor–acceptor heterojunctions.[35,36] The structures of the non-fullerene SMA DTBCIC series are shown in Fig. 1, where dithienobenzothiadiazol (DTBT) is used as an intermediate C unit to overcome the poor planarity problem[37,38] and 4,4-bis(2-ethylhexyl)-4H-cyclopenta[2,1-b:3,4-b′] dithiophene (CPDT) and 2-(3-oxo-2,3-dihydro-1H-inden-1-ylidene) malononitrile (IC) are applied as the donor and acceptor module units, respectively. Fluorine and chlorine atoms are introduced to terminal IC groups to obtain DTBCIC-F and DTBCIC-Cl NFAs, respectively. Based on density functional theory (DFT) and time-dependent density functional theory (TD-DFT), the structural properties (bond lengths and angles, frontier molecular orbitals (FMOs)), electrochemical parameters (ionization potential (IP), electron affinity (EA), chemical hardness and recombination energy), absorption spectra and properties of some excited states for their compounds are investigated. Furthermore, to clarify charge separation efficiency in OSCs, the exciton dissociation rate and charge reorganization rate of the interface and charge mobility of the dimer stack are calculated and analyzed, respectively. The interaction of D/A and its influence on the charge transfer process are explained by calculating the surface electrostatic potential (ESP). Finally, photovoltaic parameters of heterojunction solar cells based on these donors and acceptors are theoretically investigated. The results show that the designed Ce_6Me_3/DTBCIC-Cl interface has a better photoelectric performance than the others, and is expected to become a promising active layer material to upgrade the properties of chlorophyll-based OSCs.

2. Methods

The chemical structures of the Ce_6Me_3, $PC_{71}BM$ and DTBCIC molecules were optimized using DFT[39,40] with the Becke three-parameter exchange functional and the gradient-corrected functional of Lee–Yang–Parr (B3LYP)[41,42] and the 6-31G(d) basis set.[43] Then, frequency analysis[44,45] was done to ensure that the optimized geometries are energy-minimum points without imaginary frequencies.[46] From the optimized structures of the ground states, all investigated molecular relative bond lengths, dihedral angles and FMOs were calculated. From the optimized results of the anion/cation states, the EAs and IPs can also be obtained. TD-DFT[47] with the Coulomb-attenuated method (CAM)-B3LYP functional[48] and 6-31G(d) basis set was utilized to acquire the data related to the photoexcitation characteristics, including the oscillator strengths, electronic transition energies and contribution of the major molecular orbitals. Subsequently, all molecular hole/electron mobilities could be computed successfully by optimizing the constructed dimer structures at the PW91PW91[49]/6-31G(d) level. For the calculation of mobility, another method considering the phase state was also used, mainly based on molecular dynamics, to generate the amorphous structures of the NFAs; then the charge transport ability could be analyzed with the MOMAP software package.[50,51] The charge transfer integral between nearest-neighbor molecules was calculated and the carrier mobility rate calculated based on the Marcus theory. According to this rate, under the theoretical framework of charge random walk, the mobility of materials in all directions is further calculated by the Monte Carlo statistical method.[52,53] Finally, the geometric optimization of the four interfaces

(Ce_6Me_3/$PC_{71}BM$, Ce_6Me_3/DTBCIC-H, Ce_6Me_3/DTBCIC-F and Ce_6Me_3/DTBCIC-Cl) was implemented through the wB97XD[54]/6-31G(d) level, and the light absorption properties of the interfaces can be obtained utilizing TD-DFT. All these simulations were carried out in a chloroform solution and performed using the Gaussian 09 program package.[55,56] In addition, by using the Multiwfn 3.8 package,[57,58] the density of states (DOS) and electronic excitation could be analyzed.[59,60] We also obtained the charge difference density (CDD)[54] and electrostatic surface potential (ESP)[61] of the investigated molecules.

3. Results and discussion

3.1. Molecular structures and FMOs

All investigated molecules, including the Ce_6Me_3 donor, the fullerene acceptor $PC_{71}BM$ and the DTBCIC series NFAs, were optimized. These optimized structures are all minimum points rather than saddle points on their corresponding potential energy surfaces.[44] Their geometric configurations are shown in Fig. 1, where a single line indicates that there is a single bond between two atoms, two plain lines indicate that there is a double bond between two atoms, and a flat line and a dashed line indicate a conjugated double bond, i.e., two double bonds separated by a single bond.

The molecular structural parameters of the NFAs were calculated, and the corresponding data are listed in Table S1. Fluorination and chlorination of the capping groups have a minimal effect on the bond lengths between the molecular acceptor, donor and center units for the DTBCIC series. For instance, the L4–L5 bond lengths of these NFAs between the IC and the CPDT are 1.412 Å, 1.410 Å and 1.408 Å, respectively, and their L6–L7 bond lengths between the CPDT unit and DTBT central core are 1.440 Å. By comparing these molecular dihedral angles, it is found that the symmetry on both sides of the molecules is almost unchanged after fluorination and chlorination. For DTBCIC-H, the molecular angles of θ_1 and θ_6, θ_2 and θ_5, and θ_3 and θ_4 have extremely close torsional angles, and those of DTBCIC-F and DTBCIC-Cl show the same trend. The dihedral angles $\theta_1/\theta_2/\theta_3$ are 0.087°/0.182°/6.209° (DTBCIC-H), 0.061°/0.044°/5.479° (DTBCIC-F) and 0.033°/0.034°/5.468° (DTBCIC-Cl), respectively. The lower HOMO–LUMO bandgap value may come from a lesser dihedral angle.[62] Among these molecules, DTBCIC-Cl has stronger flatness and tighter packing and may have a smaller energy gap. This would be more favorable for the charge transport process and could potentially improve various optoelectronic properties.

Table 1 shows the results of the theoretical calculations for the energy levels of the FMOs. The HOMOs of Ce_6Me_3, $PC_{71}BM$, DTBCIC-H, DTBCIC-F and DTBCIC-Cl are −5.13 eV, −5.57 eV, −5.23 eV, −5.28 eV and −5.31 eV, respectively, and their LUMOs are −2.65 eV, −3.04 eV, −3.32 eV, −3.39 eV and −3.45 eV, respectively. This result exhibits a matching trend with the experimental values,[35,36] suggesting the feasibility of the theoretical research method. The HOMO and LUMO of Ce_6Me_3 are above those of all investigated acceptors, implying successful exciton dissociation at the D/A interfaces. This condition is necessary for the acceptor and donor molecules to form bulk heterojunctions that satisfy the OSC mechanism.[63] Regarding the influence of chlorination on the LUMOs, it is found that the LUMOs of the acceptors are arranged in the order DTBCIC-H > DTBCIC-F > DTBCIC-Cl, meaning that the chlorinated DTBCIC-Cl has the deepest LUMO level. A lowered LUMO level can make the system more stable and facilitate the injection of electrons, but may also yield reduced optoelectronic parameters, such as open-circuit voltage (V_{OC}).[27] Because of its higher LUMO, the fullerene acceptor has a higher V_{OC} than NFA molecules. The order of the energy gaps of the acceptors is $PC_{71}BM$ (2.53 eV) > DTBCIC-H (1.91 eV) > DTBCIC-F (1.89 eV) > DTBCIC-Cl (1.86 eV). The smaller the energy gap is, the easier it is for electrons to be excited to the LUMO, which is more conducive to obtaining higher chemical reactivity and photon utilization.[64,65]

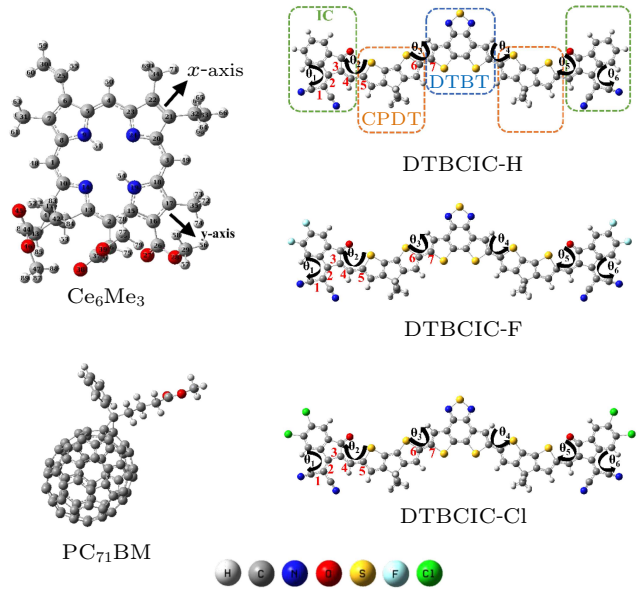


Fig. 1. Optimized chemical structures of the Ce_6Me_3 donor and all investigated acceptors ($PC_{71}BM$, DTBCIC-H, DTBCIC-F, DTBCIC-Cl) and color labels for different atoms.

Table 1. The energy levels of frontier molecular orbitals and the Δ_{H-L} of all investigated molecules (eV).

Molecule	HOMO	LUMO	Δ_{H-L}	HOMO[a]	LUMO[a]
Ce_6Me_3	–5.13	–2.65	2.48	–5.20	–3.60
$PC_{71}BM$	–5.57	–3.04	2.53		
DTBCIC-H	–5.23	–3.32	1.91	–5.55	–3.71
DTBCIC-F	–5.28	–3.39	1.89	–5.59	–3.82
DTBCIC-Cl	–5.31	–3.45	1.86	–5.62	–3.87

[a]Data are experimental values from Refs. [35,36].

FMOs are the most interesting molecular orbitals because they are essential for understanding the process of charge transfer. The FMOs of all five molecules and the position of their electron delocalization on the molecules are presented in Fig. 2. The HOMO of Ce_6Me_3 is relatively uniformly distributed over the entire π-conjugated skeleton, while the LUMO is mostly concentrated on both sides of the y-axis. For the NFAs, the HOMOs mainly exist in the central and donor units of the conjugated main chain. However, their LUMO density is focused on the entire main molecular skeleton, thereby revealing the direction of charge transfer within the molecule. We performed DOS analysis on the three NFA molecule polymers, as shown in Fig. S1. The DOS diagrams include the total density of states and partial density of states (PDOS), which can be used to estimate the contribution of each group to the molecular orbitals.[66,67] It can be observed that the contribution to the HOMO mainly comes from the donor unit (CPDT). In contrast, the contribution to the LUMO is more from the acceptor unit (IC). The detailed contribution rates of the CPDT, IC and central unit (DTBT) to the HOMOs and LUMOs were also calculated and are depicted in Table S2. These specific results are generally consistent with those mentioned above. For the HOMO orbital, the donor units of all molecules contribute about 50%; and for the LUMO, the acceptor groups also contribute about 50%.

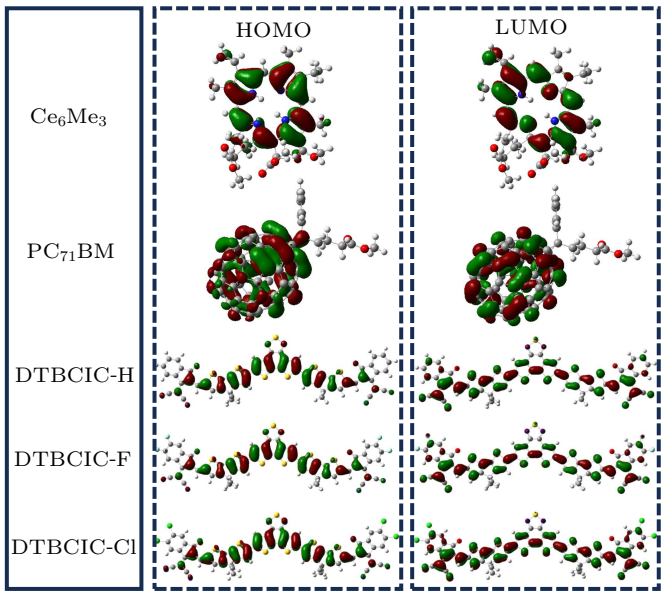


Fig. 2. The FMOs (HOMOs and LUMOs) of all investigated molecules.

3.2. Characterization of electrochemical parameters

Various important electrochemical parameters of these five molecules are presented in Table 2, including IPs, EAs, the electrophilicity index (ω), absolute hardness (η) and reorganization energy. The IPs and EAs are necessary parameters for predicting the charge transport ability of molecules.[68,69] A lower IP makes the process of ionizing electrons easier, while a higher EA results in easier access to electrons, thereby reflecting a stronger electron transport capability.[28] IPs and EAs may be gained through the energy difference between the optimized neutral and ionic (cation/anion) structure of a molecule, respectively. The IPs of Ce_6Me_3, $PC_{71}BM$, DTBCIC-H, DTBCIC-F and DTBCIC-Cl are 5.17 eV, 5.63 eV, 5.19 eV, 5.24 eV and 5.27 eV, respectively, and their EA values take the order of DTBCIC-Cl (3.46 eV) > DTBCIC-F (3.40 eV) > DTBCIC-H (3.33 eV) > $PC_{71}BM$ (3.01 eV) > Ce_6Me_3 (2.66 eV). According to Koopmans' approximation theorem,[70] the IP and EA are approximately equal to the value of HOMO and LUMO energy, respectively, which is consistent with the above calculation results. After chlorine atom substitution, DTBCIC-Cl has a higher EA than the other molecules and also has better electron injection efficiency. In addition, the IP and EA of the Ce_6Me_3 molecule are smaller, thereby allowing for smoother electron transport from donor to acceptor and indicating that it has good donor characteristics.

Table 2. The electrochemical parameters including ionization potential IP (eV), electron affinity EA (eV), electrophilicity index ω, absolute hardness η (eV) and reorganization energy (eV) of all investigated molecules.

Molecule	IP	EA	ω	η	λ_h	λ_e
Ce_6Me_3	5.17	2.66	6.12	1.25	0.184	0.271
$PC_{71}BM$	5.63	3.01	7.12	1.31	0.110	0.180
DTBCIC-H	5.19	3.33	9.76	0.93	0.178	0.135
DTBCIC-F	5.24	3.40	10.14	0.92	0.177	0.129
DTBCIC-Cl	5.27	3.46	10.53	0.90	0.176	0.118

The higher the ω of a molecule the better its electrophilicity and electron-withdrawing ability are.[71] As shown in Table 2, the ω values of all investigated molecules are 6.12, 7.12, 9.76, 10.14 and 10.53, respectively. Therefore, DTBCIC-Cl, which has the highest value, may have better electron-withdrawing properties. In addition, the stability of molecules is also a significant factor for judging the performance of materials. Absolute hardness (η) is a major parameter for estimating molecular charge transfer stability. Generally, the smaller the absolute hardness, the easier the charge transfer.[27] Furthermore, DTBCIC-Cl has a lower η value (0.90 eV) than the other acceptors (0.93 eV for DTBCIC-H, 0.92 eV for DTBCIC-F and 1.31 eV for $PC_{71}BM$), illustrating that it has reduced resistance to charge transfer due to the substitution of chlorine.

According to the theory of Marcus, the reorganization energy can usually be adopted to predict the molecular transport capacity.[72] The molecular reorganization energy may be composed of both internal and external components.[73,74] Usually, because of the complex interactions between solute and dissolvent molecules, it is difficult to evaluate the external

recombination energy. Therefore, in this work, only the internal part can be considered and discussed; this consists of λ_h (the reorganization energy of the hole) and λ_e (the reorganization energy of the electron)[75,76]

$$\lambda_h = E_0^+ - E_+ + E_+^0 - E_0, \quad (1)$$

$$\lambda_e = E_0^- - E_- + E_-^0 - E_0, \quad (2)$$

where E_0^+ (E_0^-) is the energy of cation (anion) under the neutral structure, E_- (E_+) is the energy after optimizing the structure of the anion/cation, E_-^0 (E_+^0) is the neutral energy calculated based on the geometric structure of the ion and E_0 represents the energy of the neutral structure.

The calculations, including the neutral and ionic geometric optimization and single-point calculations, were performed by employing DFT at the B3LYP and 6-31G(d) level. The values of λ_h for Ce_6Me_3, $PC_{71}BM$, DTBCIC-H, DTBCIC-F and DTBCIC-Cl are 0.184 eV, 0.110 eV, 0.178 eV, 0.177 eV and 0.176 eV, respectively, as shown in Table 2. The NFAs have approximate λ_h values, which means that they have similar hole transport abilities. The λ_e of the investigated molecules follow the order Ce_6Me_3 (0.271 eV) > $PC_{71}BM$ (0.180 eV) > DTBCIC-H (0.135 eV) > DTBCIC-F (0.129 eV) > DTBCIC-Cl (0.118 eV), so DTBCIC-Cl has a lower λ_e. It was also found that the NFAs may be more capable than fullerenes of being excellent electron transport materials. Furthermore, after the introduction of chlorine atoms, the NFAs had a higher electron transfer ability, which is beneficial to improving the photocurrent and PCE of organic solar cells.

3.3. Molecular excited properties

TD-DFT was used to investigate the light absorption characteristics of all molecules. As displayed in Fig. 3(a), the molecular absorption spectrum of Ce_6Me_3 was observed with the Soret band at ~ 400 nm (strong absorption peak), due to the formation of a sizeable delocalized π bond through the $\pi \rightarrow \pi^*$ transition, and the Q_y band at 600–700 nm (weak absorption peak), in agreement with the experimental results.[35,77] $PC_{71}BM$ was found to have strong light absorption in the ultraviolet range. DTBCIC-Cl has a larger absorption peak wavelength and extinction coefficient than the other acceptors, suggesting that it could be a more efficient acceptor because the strong and broad absorption should provide the corresponding OSC with better light-harvesting ability, especially in the near-infrared region. This suggests that there is a good absorption complementarity with the Ce_6Me_3 donor, which is beneficial to the light capture of chlorophyll-based OSCs.

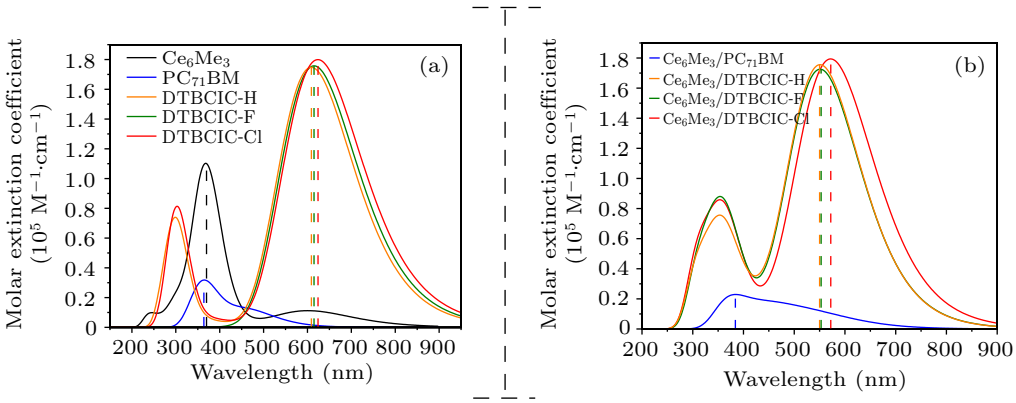


Fig. 3. The UV–vis absorption spectra of (a) all investigated molecules and (b) the four D/A interfaces.

Table 3 shows the relevant spectral performance parameters, including absorption wavelength, oscillator strength and excitation energy, together with the major contributing orbitals of all investigated donor and acceptors from the S_1 to S_5 excited states. Other excited state properties are given in Tables S3–S7. Strong absorption peaks are located at 373.91 nm (Ce_6Me_3), 386.71 nm ($PC_{71}BM$), 609.65 nm (DTBCIC-H), 615.92 nm (DTBCIC-F) and 624.42 nm (DTBCIC-Cl). In contrast, a more significant red shift absorption of 237.71 nm was observed from the fullerene acceptor $PC_{71}BM$ to DTBCIC-Cl. The spectral redshifts of DTBCIC-Cl relative to DTBCIC-H and DTBCIC-F are 14.77 nm and 8.50 nm, respectively, implying a higher electronegativity of non-fullerene compared with fullerene acceptors and the enhanced vital electron-withdrawing ability and close-packed stacking of chlorinated rather than fluorinated NFAs. Therefore, DTBCIC-Cl may have greater potential to obtain a higher short-circuit current (J_{SC}) in OSCs as an acceptor.

Figure S2 shows the CDD plots of DTBCIC-H, DTBCIC-F and DTBCIC-Cl from S_1 to S_5, which can be used to identify the electron density change in every excited state.[66] It can be seen that the process of electron transfer is mainly from the molecular backbone to the electron-withdrawing IC groups at both ends. The contributions of various groups in the NFAs to electrons and holes and their corresponding heat maps are shown in Fig. S3. The IC units at both ends of the main chain

are set as fragment 1, the CPDT units as fragment 2 and the DTBT central group as fragment 3. From the color difference of the heat maps, the color corresponding to the hole contribution rates of the three molecules has an identical distribution, and most comes from the DTBT unit of fragment 2. However, for the electron contribution, the DTBCIC-Cl molecule is significantly darker in fragment 1 than the other two molecules. This is consistent with the data on fragment contribution rates. The contribution rate of fragment 1 to electrons is DTBCIC-H (39.21%) < DTBCIC-F (40.39%) < DTBCIC-Cl (42.13%), meaning that the above results are consistent with the CDD analysis, further proving that the IC group introduced with chlorine atom has a stronger electron-withdrawing property.

Table 3. The excitation energy, absorption wavelength λ_{ab}, oscillator strength f and major contribution MOs of all investigated molecules (S_1–S_5).

Molecule	State	Transition energy (eV/nm)	Oscillator strength f	Contribution MO
Ce_6Me_3	S_1	2.0293/610.97	0.2558	H→L/0.64207
	S_2	2.4442/507.26	0.0563	H-1→L/0.39696
	S_3	3.3159/373.91	1.4505	H→L+1/0.57894
	S_4	3.3930/365.42	1.1838	H-1→L+1/0.60590
	S_5	3.6510/339.59	0.1319	H-2→L/0.62763
$PC_{71}BM$	S_1	2.2650/547.39	0.0068	H→L/0.51697
	S_2	2.4371/508.73	0.0462	H→L+1/0.55567
	S_3	2.6029/476.34	0.0400	H→L+2/0.59043
	S_4	2.6508/467.73	0.0348	H-1→L/0.57184
	S_5	2.7020/458.86	0.0753	H-1→L+1/0.55852
DTBCIC-H	S_1	2.0337/609.65	4.2708	H→L/0.58305
	S_2	2.3084/537.10	0.0704	H→L+1/0.48750
	S_3	2.8820/430.21	0.0215	H→L+2/0.48959
	S_4	3.1792/389.99	0.0124	H→L+3/0.43224
	S_5	3.2346/383.31	0.0628	H→L+4/0.45875
DTBCIC-F	S_1	2.0130/615.92	4.2970	H→L/0.58121
	S_2	2.2857/542.44	0.0684	H→L+1/0.48833
	S_3	2.8670/432.46	0.0101	H→L+2/0.47567
	S_4	3.1033/399.53	0.0120	H→L+3/0.44315
	S_5	3.1677/391.41	0.0773	H→L+4/0.44780
DTBCIC-Cl	S_1	1.9856/624.42	4.4064	H→L/0.57910
	S_2	2.2553/549.76	0.0580	H→L+1/0.48817
	S_3	2.8547/434.32	0.0048	H→L+2/0.45533
	S_4	3.0640/404.65	0.0252	H→L+3/0.45004
	S_5	3.1310/395.99	0.0828	H→L+4/0.42828

3.4. Properties of D/A compounds

To further study the photovoltaic characteristics of chlorophyll-based OSCs, we designed three D/A interfaces based on the chlorophyll derivative and NFAs, and carried out theoretical simulations and a performance comparison with the experimental $Ce_6Me_3/PC_{71}BM$ interface. Figure 4 displays the ground state optimized structures of the $Ce_6Me_3/PC_{71}BM$, Ce_6Me_3/DTBCIC-H, Ce_6Me_3/DTBCIC-F and Ce_6Me_3/DTBCIC-Cl interfaces, and Table 4 contains data for the FMOs and energy gaps. For the HOMOs of all D/A interfaces, electron delocalization occurs on the Ce_6Me_3 donor, and for the LUMOs it is mainly concentrated on the acceptors. The energy gaps of these interfaces present the trend $Ce_6Me_3/PC_{71}BM$ (5.03 eV) > Ce_6Me_3/DTBCIC-H (5.01 eV) > Ce_6Me_3/DTBCIC-F (4.88 eV) > Ce_6Me_3/DTBCIC-Cl (4.85 eV). A smaller band gap can facilitate the process of photoelectric conversion. Thus, Ce_6Me_3/DTBCIC-Cl is more conducive to obtaining a higher J_{SC}.

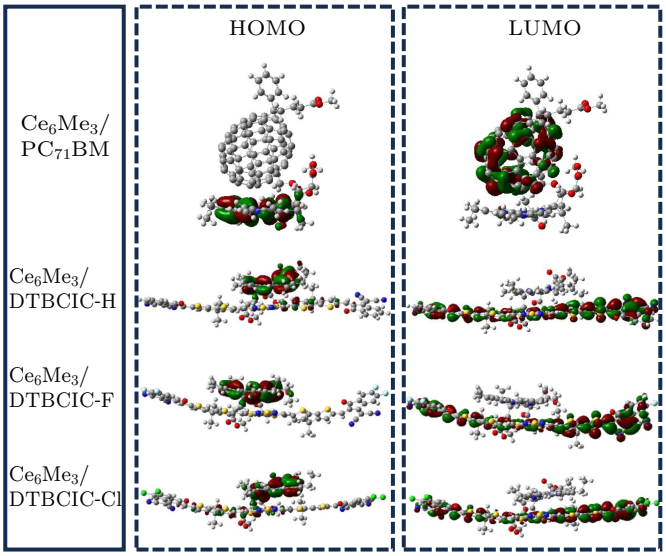


Fig. 4. The FMOs of four complexes.

Table 4. The HOMO and LUMO energy levels and energy gaps of the four investigated D/A interfaces (eV).

D/A interfaces	HOMO	LUMO	Δ_{H-L}
$Ce_6Me_3/PC_{71}BM$	–6.69	–1.66	5.03
Ce_6Me_3/DTBCIC-H	–6.79	–1.78	5.01
Ce_6Me_3/DTBCIC-F	–6.74	–1.86	4.88
Ce_6Me_3/DTBCIC-Cl	–6.78	–1.93	4.85

In addition, to quantify the specific contributions of donors and acceptors to interface FMOs, their DOS are drawn in Fig. 5. By analyzing the DOS, Ce_6Me_3 mainly contribute to the HOMOs and the $PC_{71}BM$ and DTBCIC acceptors mainly contribute to the LUMOs. The corresponding contribution rates were calculated and are shown in Fig. 5. The contribution rates of Ce_6Me_3 to the HOMOs of the four interfaces are 98.55% for $Ce_6Me_3/PC_{71}BM$, 90.63% for Ce_6Me_3/DTBCIC-H, 97.57% for Ce_6Me_3/DTBCIC-F and 87.15% for Ce_6Me_3/DTBCIC-Cl, respectively. In contrast, the Ce_6Me_3 contribution rates to the LUMOs of the investigated interfaces are 3.76%, 1.06%, 0.39% and 0.53%, respectively. It can be seen that the fullerene acceptor $PC_{71}BM$ had a lower contribution to the HOMOs and LUMOs of the D/A interfaces than the NFAs.

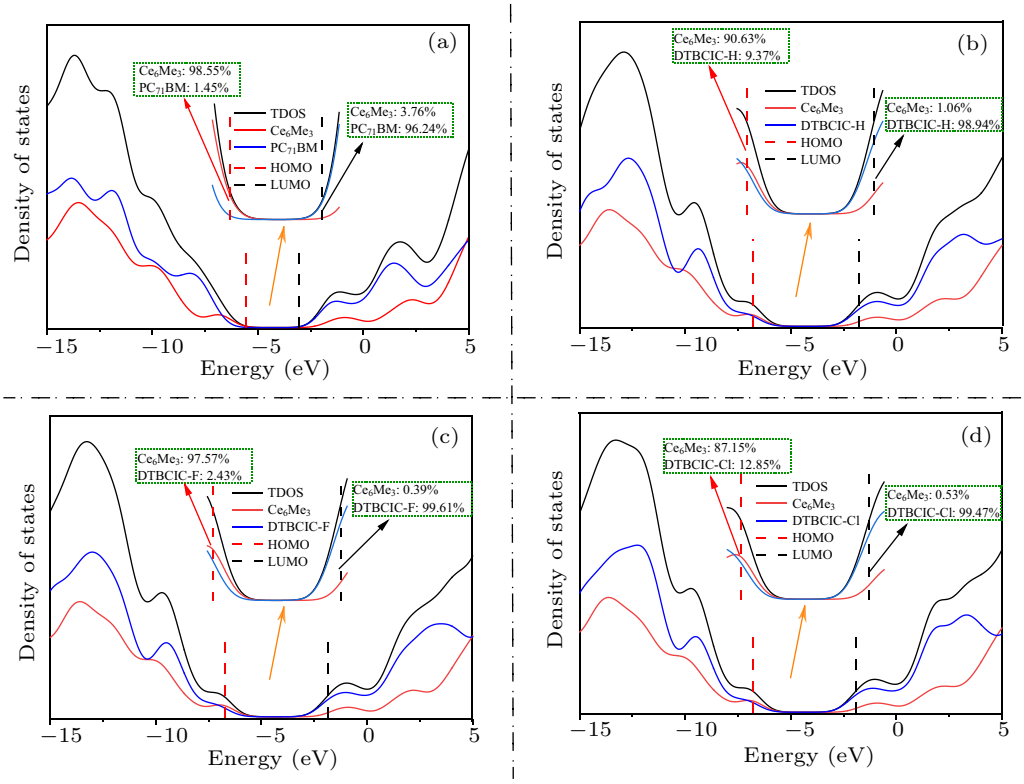


Fig. 5. The density of states (DOS/PDOS) of the four interfaces: (a) $Ce_6Me_3/PC_{71}BM$, (b) Ce_6Me_3/DTBCIC-H, (c) Ce_6Me_3/DTBCIC-F, (d) Ce_6Me_3/DTBCIC-Cl.

3.5. Excited characteristics of the compounds

Absorption spectra of $Ce_6Me_3/PC_{71}BM$, Ce_6Me_3/DTBCIC-H, Ce_6Me_3/DTBCIC-F and Ce_6Me_3/DTBCIC-Cl are presented in Fig. 3(b). For the D/A interface based on $PC_{71}BM$, the optical absorption range is 300–800 nm. For the compound incorporated with NFAs, the spectral range is 200–900 nm, which is more beneficial for broadening the spectra and increasing the absorption of visible, near-ultraviolet and infrared light. The spectrum of Ce_6Me_3/DTBCIC-Cl has a larger redshift compared with Ce_6Me_3/DTBCIC-F and Ce_6Me_3/DTBCIC-H, suggesting that this D/A compound will have a better photovoltaic performance in solar cells.

The relational parameters are also listed in Table 5 and Tables S8–S11. The wavelengths of the first absorption peaks show the trend $Ce_6Me_3/PC_{71}BM$ (371.71 nm) < Ce_6Me_3/DTBCIC-H (554.39 nm) < Ce_6Me_3/DTBCIC-F (556.90 nm) < Ce_6Me_3/DTBCIC-Cl (575.04 nm). In addition, the HOMO→LUMO+4 orbital transition is the main approach for the peak of the fullerene acceptor compound $Ce_6Me_3/PC_{71}BM$. The other acceptor admixture peaks are all shown to be from the HOMO–1→LUMO transition. The parallel oscillator strengths of the four interfaces are 0.2217, 3.9836, 3.4272 and 4.1603, respectively. It can be observed that Ce_6Me_3/DTBCIC-Cl has excellent light absorption properties, demonstrating that the chlorination of acceptor molecules is a feasible strategy for enhancing the photoexcitation performance of chlorophyll-based OSCs.

Table 5. The light absorption properties including excitation energy, absorption wavelength λ_{ab}, oscillator strength f and main contribution orbit of the stronger excited states of all investigated compounds.

Molecule	State	Transition energy (eV/nm)	Oscillator strength f	Contribution MO
$Ce_6Me_3/PC_{71}BM$	S_1	2.2056/562.12	0.1730	H→L+3/0.56574
	S_6	2.6871/461.40	0.0740	H-2→L+2/0.55991
	S_9	2.7713/447.38	0.0706	H-3→L+1/0.29821
	S_{11}	2.8044/442.10	0.0655	H-2→L+1/0.28413
Ce_6Me_3/DTBCIC-H	S_1	2.2364/554.39	3.9836	H-1→L/0.46171
	S_2	2.3059/537.68	0.2090	H→L+2/0.60227
	S_4	2.6113/474.79	0.1407	H-2→L+2/0.50895
	S_5	2.8329/437.66	0.0267	H→L/0.52534
Ce_6Me_3/DTBCIC-F	S_1	2.2263/556.90	3.4272	H-1→L/0.44969
	S_2	2.2625/547.99	0.5094	H→L+2/0.62038
	S_3	2.4477/506.54	0.3786	H-3→L/0.47493
	S_{11}	3.2851/377.41	0.1298	H→L+5/0.42087
Ce_6Me_3/DTBCIC-Cl	S_1	2.1561/575.04	4.1603	H-1→L/0.47562
	S_2	2.2753/544.91	0.1438	H→L+2/0.54745
	S_4	2.5713/482.19	0.1261	H-2→L+2/0.49578
	S_9	3.1469/393.99	0.0047	H→L+1/0.49070

The CDD of the excited state of the four compounds not only reveals the function of each group for light absorption but also the charge transfer process,[66] which is convenient for subsequent research and analysis. The CDD plots of some strongly excited states are shown in Fig. 6, with other states (S_1–S_{15}) depicted in Figs. S4–S7. Observation and analysis of all the CDDs from S_1 to S_{15} shows that they can be divided into three types as follows: (1) Most electrons and holes are situated on the donor Ce_6Me_3; for instance, S_1 for $Ce_6Me_3/PC_{71}BM$, S_2 and S_4 for Ce_6Me_3/DTBCIC-H, S_2 for Ce_6Me_3/DTBCIC-F and S_2 and S_4 for Ce_6Me_3/DTBCIC-Cl, revealing that localized ex-

citation and intramolecular charge transfer take place only at the donor. (2) The holes are situated on the donor and the electrons focused on the acceptor, implying that intermolecular charge transfer (ICT) is a process involving holes to the donor and electrons to the acceptor. Near-complete charge separation can be observed with ICT, which has a significant impact on the performance analysis of OSCs, such as S_9, S_5, S_{11} and S_9 for $Ce_6Me_3/PC_{71}BM$, Ce_6Me_3/DTBCIC-H, Ce_6Me_3/DTBCIC-F and Ce_6Me_3/DTBCIC-Cl, respectively. (3) For S_6 of $Ce_6Me_3/PC_{71}BM$ and S_1 of Ce_6Me_3/DTBCIC series, most holes and electrons are distributed on receptors, suggesting that charge transfer occurs merely at the acceptor. Consequently, CDDs can intuitively give the charge increases and decreases as well as the distribution of charges on each molecule, which is beneficial to the analysis of exciton dissociation at the interface.

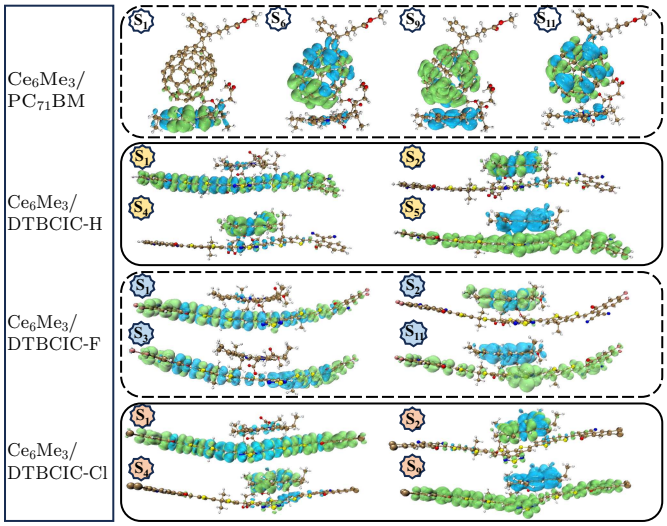


Fig. 6. The CDD of the stronger excited states of the four compounds, where the green and blue colors stand for the electron and hole, respectively.

3.6. Analysis of surface electrostatic potential and interfacial charge transfer

To consider the potential influence of D/A interaction on heterojunction and photovoltaic performance, we analyzed the impact of the D/A system on charge transfer based on the molecular surface electrostatic potential (ESP).[78,79] The ESP of all the investigated molecules is shown in Fig. 7, and the relevant quantitative information is listed in Table S12. From Fig. 7, it can be seen that the NFAs exhibit most of the red regions in the intermediate groups and have an overall positive ESP distribution, which is also consistent with the greater positive surface area values and the overall average electrostatic potential values shown in Table S12. Comparing the three NFAs, there are more blue regions near the chlorine atom in the terminal group of DTBCIC-Cl, indicating that the end cap of DTBCIC-Cl has stronger electron-absorbing ability. The overall average electrostatic potential of the acceptor molecules is 1.48 kcal·mol^{-1} for $PC_{71}BM$, 4.32 kcal·mol^{-1} for DTBCIC-H, 5.92 kcal·mol^{-1} for DTBCIC-F and 6.01 kcal·mol^{-1} for DTBCIC-Cl. The donor molecule Ce_6Me_3 has a relatively lower ESP distribution (0.40 kcal·mol^{-1}), which is due to its high electron density. Therefore, it is easy to find that the differences in ESP between donor and acceptor molecules are 1.08 kcal·mol^{-1} ($Ce_6Me_3/PC_{71}BM$), 3.92 kcal·mol^{-1} (Ce_6Me_3/DTBCIC-H), 5.52 kcal·mol^{-1} (Ce_6Me_3/DTBCIC-F) and 5.61 kcal·mol^{-1} (Ce_6Me_3/DTBCIC-Cl). This shows that the Ce_6Me_3/DTBCIC-Cl system has the strongest D/A interaction: the corresponding intermolecular electrostatic field offers the power for exciton separation, which enhances the charge transfer process and gives it higher charge mobility.[80,81]

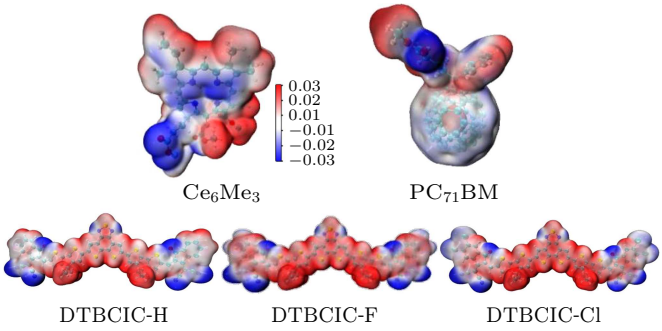


Fig. 7. Surface electrostatic potential diagrams (red and blue indicate positive and negative electrostatic potential, respectively).

Charge separation at the D/A interface significantly affects solar cell performance. Generally, the process can be understood in two steps, namely, separation into electron–hole pairs with a strong binding force then changing into free electrons and holes.[82] To efficiently separate excitons it is necessary to overcome the large exciton binding energy, primarily due to the Coulomb attraction between electrons and holes.[83] Therefore, E_b can be assessed by the Coulomb attraction energy (E_C),[57,58] which is based on expression (atomic unit system)[84,85]

$$E_C = \iint \frac{\rho^{hole}(r_1)\rho^{ele}(r_2)}{|r_1 - r_2|} dr_1 r_2, \tag{3}$$

where ρ^{ele} and ρ^{hole} represent the electron and hole densities of the transition orbitals, respectively, and r_1 and r_2 are the charge coordinates; E_b is the negative number of E_C.

According to the above CDDs of all investigated compounds, we can obtain the complete ICT states and their Coulomb attraction energies, listed in Table 6, which are −1.800 eV for S_9 of $Ce_6Me_3/PC_{71}BM$, −1.714 eV for S_5 of Ce_6Me_3/DTBCIC-H, −1.695 eV for S_{11} of Ce_6Me_3/DTBCIC-F and −1.452 eV for S_9 of Ce_6Me_3/DTBCIC-Cl. These data indicate that $Ce_6Me_3/PC_{71}BM$ may need to overcome a larger Coulomb attraction energy to make exciton dissociation more complete.

Ce_6Me_3/DTBCIC-Cl, with a lower E_C, will allow for easier exciton separation, resulting in a higher J_{SC}.

Table 6. The dipole moment difference $\Delta\mu$ (a.u.), transition dipole moment μ_{tr} (a.u.), vertical excitation energy ΔE (eV), electron coupling V_{DA} (eV) and Coulomb attractive energy E_C (eV) of the ICT states of the D/A interfaces.

D/A interface	State	$\Delta\mu$	μ_{tr}	ΔE	V_{DA}	E_C
Ce_6Me_3/$PC_{71}BM$	S_9	–2.7095	1.0199	2.77	0.833	–1.800
Ce_6Me_3/DTBCIC-H	S_5	–5.2680	0.6200	2.83	0.325	–1.714
Ce_6Me_3/DTBCIC-F	S_{11}	–1.6950	1.2701	3.29	1.366	–1.695
Ce_6Me_3/DTBCIC-Cl	S_9	0.7900	0.2475	3.15	0.835	–1.452

When exciton dissociation takes place at the heterojunction interface it will make a significant contribution to device efficiency if the rate of charge transfer is higher than charge reorganization. These two rates at the interface are usually estimated using the Marcus theory and are expressed as[86,87]

$$K = \sqrt{\frac{4\pi^3}{\hbar^2\lambda k_B T}}|V_{DA}|^2 \exp\left(-\frac{(\Delta G+\lambda)^2}{4\lambda k_B T}\right), \tag{4}$$

where ΔG is the Gibbs free energy change, K represents the rate and the constant terms $\hbar$, k_B and T are Planck's constant, Boltzmann's constant and temperature (300 K), respectively. λ is the reorganization energy of the compound. V_{DA} is the charge transfer integral, which may be evaluated by utilizing the recognized Mulliken–Hush model of two states[10,88–90]

$$V_{DA} = \frac{\mu_{tr}\Delta E}{\sqrt{(\Delta\mu)^2+4(\mu_{tr})^2}}, \tag{5}$$

where μ_{tr} is the transition dipole moment, which can be assessed by the electron dipole moment of the initial state and the complete ICT state[88]

$$\mu_{tr} = \sqrt{x^2+y^2+z^2}. \tag{6}$$

The ΔE represents the vertical excitation energy of the ICT state and $\Delta\mu$ reflects the difference in dipole moment, which is usually evaluated through the finite field difference method.[86] These parameters of the complete ICT states (S_9, S_5, S_{11} and S_9 for Ce_6Me_3/$PC_{71}BM$, Ce_6Me_3/DTBCIC-H, Ce_6Me_3/DTBCIC-F and Ce_6Me_3/DTBCIC-Cl, respectively) were calculated and are shown in Table 6. Their V_{DA} values are found to be 0.833 eV, 0.325 eV, 1.366 eV and 0.835 eV, respectively.

The recombination energy of an interface includes both the external recombination energy λ_o and the internal recombination energy λ_i. Because it is challenging to calculate λ_o theoretically, a value of 0.5 eV is used here for the results of the recombination energy study in the experiment.[91] The expression for λ_i of the interface is[75,92]

$$\lambda_i = E_0^+(\mathrm{D}) - E_+(\mathrm{D}) + E_-^0(\mathrm{A}) - E_0(\mathrm{A}), \tag{7}$$

where $E_0^+(\mathrm{D})$ is the neutral structural energy of the donor molecule carrying a positive charge, $E_+(\mathrm{D})$ is the optimized donor cation structural energy, $E_-^0(\mathrm{A})$ is the energy of the anion structure of the acceptor without charge and $E_0(\mathrm{A})$ is the energy of the neutral acceptor.

The changes in free energy during charge recombination and exciton separation are denoted as ΔG_{CR} and ΔG_{CS}, respectively. The expression for ΔG_{CR} is[93]

$$\Delta G_{CR} = E_{IP}(\mathrm{D}) - E_{EA}(\mathrm{A}). \tag{8}$$

The equation for ΔG_{CS} is[94]

$$\Delta G_{CS} = -\Delta G_{CR} - E_{D1} + E_C, \tag{9}$$

where E_{D1} refers to the excitation energy of the donor molecule's lowest singlet state and E_C represents the Coulomb interaction energy of the ICT state. It is noteworthy that the values of the Gibbs free energy are all negative. This information is displayed in Table 7.

Table 7. The reorganization energy λ (eV), Gibbs free energy change of charge recombination ΔG_{CR} (eV) and Gibbs free energy charge of exciton separation ΔG_{CS} (eV), charge reorganization rate K_{CR} (s^{-1}) and exciton separation rate K_{CS} (s^{-1}) of all investigated D/A interfaces.

D/A interface	λ_i	λ	ΔG_{CR}	ΔG_{CS}	K_{CR}	K_{CS}	K_{CS}/K_{CR}
Ce_6Me_3/$PC_{71}BM$	0.181	0.681	–2.159	–1.930	4.753×10^2	3.375×10^6	7.100×10^3
Ce_6Me_3/DTBCIC-H	0.160	0.660	–1.831	–1.516	4.085×10^6	4.723×10^{10}	1.156×10^4
Ce_6Me_3/DTBCIC-F	0.152	0.652	–1.765	–1.431	4.058×10^8	4.773×10^{12}	1.176×10^4
Ce_6Me_3/DTBCIC-Cl	0.152	0.652	–1.703	–1.126	1.110×10^9	5.166×10^{14}	4.654×10^5

The values of λ for all investigated compounds are 0.681 eV, 0.660 eV, 0.652 eV and 0.652 eV, respectively. The ΔG_{CR} values follow the order Ce_6Me_3/$PC_{71}BM$ (−2.159 eV) < Ce_6Me_3/DTBCIC-H (−1.831 eV) < Ce_6Me_3/DTBCIC-F (−1.765 eV) < Ce_6Me_3/DTBCIC-Cl (−1.703 eV). The respective ΔG_{CS} values are −1.930 eV, −1.516 eV, −1.431 eV and −1.126 eV. It can be seen from the results that Ce_6Me_3/$PC_{71}BM$ is characterized by a higher λ and absolute Gibbs free energy, implying that charge transfer at this interface will face stronger resistance and a larger free energy change for charge transfer reactions. The Ce_6Me_3/DTBCIC-Cl complex with a chlorinated NFA will have a stronger charge transfer ability than the others (see Table 7). The calculated charge reorganization rates (K_{CR}) for

Ce_6Me_3/$PC_{71}BM$, Ce_6Me_3/DTBCIC-H, Ce_6Me_3/DTBCIC-F and Ce_6Me_3/DTBCIC-Cl are 4.753×10^2 s^{-1}, 4.085×10^6 s^{-1}, 4.058×10^8 s^{-1} and 1.110×10^9 s^{-1}, respectively, and the exciton separation rates (K_{CS}) are 3.375×10^6 s^{-1}, 4.723×10^{10} s^{-1}, 4.773×10^{12} s^{-1} and 5.166×10^{14} s^{-1}, respectively. It is clear that the K_{CS} value of each of the studied complexes is larger than the K_{CR} value, which can ensure the smooth progress of the charge transfer process. The K_{CS}/K_{CR} ratio can better reflect the ability to effectively separate charges and generate a higher J_{SC}. They have the following order: Ce_6Me_3/$PC_{71}BM$ < Ce_6Me_3/DTBCIC-H < Ce_6Me_3/DTBCIC-F < Ce_6Me_3/DTBCIC-Cl. Conclusively, our theoretical findings suggest that DTBCIC-Cl is an excellent electron acceptor material for high-performance solar cells and indicate that matching chlorophyll derivatives with NFAs into heterojunctions is a feasible strategy to enhance charge transfer efficiency and thus improve the optoelectronic properties of OSCs.

3.7. Charge mobility of Ce_6Me_3 and NFAs

When the excitons undergo charge separation, the formed free electrons and holes need to move to the two poles of the solar cells through the transport layer. Therefore, charge mobility, describing the speed of movement of charge in organic molecules, plays a critical role in affecting PCE. The heat-activated hopping and continuum band models are the two main models depicting the mechanism of charge transmission.[95] The model of intermolecular hopping is selected here because of the face-to-face molecular configuration,[63] ground state optimization of which was performed under the DFT/PW91PW91/6-31G(d) level. To further study the transport characteristics of Ce_6Me_3 and the NFA materials DTBCIC-H, DTBCIC-F and DTBCIC-Cl, the Marcus theory is usually adopted to assess the hole hopping rate (k_h) and the electron hopping rate (k_e) as follows:[10,96,97]

$$k = \frac{V^2}{\hbar}\left(\frac{\pi}{\lambda k_B T}\right)^{\frac{1}{2}} \exp\left(\frac{-\lambda}{4k_B T}\right), \tag{10}$$

where V represents the transfer integral of charge, consisting of V_h and V_e, and λ expresses the hole or electron reorganization energy of the four molecules, which can be obtained from Table 2. Calculation of V is as follows:

$$V_h = \frac{E_{HOMO} - E_{HOMO-1}}{2}, \tag{11}$$

$$V_e = \frac{E_{LUMO+1} - E_{LUMO}}{2}, \tag{12}$$

where E_{HOMO}, E_{HOMO-1}, E_{LUMO} and E_{LUMO+1} are the HOMO, HOMO–1, LUMO and LUMO+1 energies of the molecule, respectively. The improved charge mobility of the molecule is due to the favorable molecular stacking with strong π–π interaction and a short accumulation distance. The following formula is commonly adopted to calculate charge mobility:[10,63]

$$\mu = \frac{er^2}{2k_B T}k, \tag{13}$$

where e is the electron charge, r represents the distance between the centroids of two adjacent molecules after stacking and k is the hopping rate.

As shown in Table 8, the hole transfer integral was larger than the electron transfer integral for the dimer of the donor material Ce_6Me_3, and there was a similar trend for the charge transfer rate as well: k_h (2.544×10^{12} s^{-1}) > k_e (8.265×10^{11} s^{-1}). The charge mobility of Ce_6Me_3 was calculated to be μ_h (0.084 $cm^2\cdot V^{-1}\cdot s^{-1}$) > μ_e (0.027 $cm^2\cdot V^{-1}\cdot s^{-1}$), demonstrating that Ce_6Me_3 can act as a sound hole transport layer and play a specific blocking role in the transport of electrons. For NFA materials, the smaller electron reorganization energy and higher electron transfer rate should be more favorable for improving the mobility of electron carriers.[27] The order of their μ_e is as follows: DTBCIC-Cl (0.902 $cm^2\cdot V^{-1}\cdot s^{-1}$) > DTBCIC-F (0.183 $cm^2\cdot V^{-1}\cdot s^{-1}$) > DTBCIC-H (0.055 $cm^2\cdot V^{-1}\cdot s^{-1}$). Compared with fluorination of DTBCIC-H, the obtained DTBCIC-Cl acceptor has better electron transmission capability, which will lead to corresponding OSCs with better optoelectronic properties. In addition, the amorphous structure of NFA molecules constructed by molecular dynamics was analyzed (see Fig. S8(a)), then the mobility of these stacked molecules can also be calculated.[98] Some three-dimensional graphs of electron migration results are shown in Fig. S8(b), illustrating that DTBCIC-H (4.901 $cm^2\cdot V^{-1}\cdot s^{-1}$) has a lower charge mobility than DTBCIC-Cl (6.182 $cm^2\cdot V^{-1}\cdot s^{-1}$), supporting the above-mentioned analysis and demonstrating that chlorine substitution (DTBCIC-Cl) can improve charge mobility and further affect J_{SC}.

Table 8. The charge transfer integrals V_e and V_h (eV), dimer distance r (Å), reorganization energies λ_e and λ_h (eV), charge transfer rates k_e and k_h (s^{-1}), hole mobility μ_h and electron mobility μ_e ($cm^2\cdot V^{-1}\cdot s^{-1}$) of dimers.

Dimer		λ_e/λ_h	V_e/V_h	k_e/k_h	μ_e	μ_h
Ce_6Me_3	4.1347	0.271/0.184	0.0188/0.0196	8.265×10^{11}/2.544×10^{12}	0.027	0.084
DTBCIC-H	4.5552	0.135/0.178	0.0105/0.0148	1.357×10^{12}/1.571×10^{12}	0.055	0.060
DTBCIC-F	4.3124	0.129/0.177	0.0195/0.0079	5.093×10^{12}/4.459×10^{11}	0.183	0.016
DTBCIC-Cl	4.5391	0.118/0.176	0.0382/0.0369	2.264×10^{13}/9.870×10^{12}	0.902	0.393

3.8. Photovoltaic properties

The most critical factor for OSC performance is to improve PCE. The valuable parameters related to the PCE are V_{OC}, J_{SC} and voltage loss (V_{LOSS}). V_{OC} can be approximated by the following empirical equation:[99]

$$V_{OC} = \frac{1}{e}|E_{HOMO}(D) - E_{LUMO}(A)| - \Delta V, \tag{14}$$

where e is the elementary charge, $E_{HOMO}(D)$ and $E_{LUMO}(A)$ are the donor's HOMO energy and the acceptor's LUMO energy, which can be found in Table 1, and ΔV is an empirical constant related to the heterojunction design, which is usually set to 0.3 V for a fullerene acceptor[100,101] and 0.5 V[86,102] for NFAs. From this equation, it can be seen that the $E_{LUMO}(A)$ is directly related to V_{OC}, and the deeper the acceptor's LUMO energy level is the lower the photoelectric parameter V_{OC} may be.

The V_{LOSS} can be estimated according to[103]

$$V_{LOSS} = \frac{E_g}{e} - V_{OC}, \tag{15}$$

where E_g represents the optical energy gap of the compound.

Usually, the following expression is used to represent J_{SC}:[86,99]

$$J_{SC} = \int \mathrm{EQE}(\lambda) S(\lambda)\, \mathrm{d}\lambda. \tag{16}$$

Considering the realistic constraint of productivity, the external quantum efficiency EQE(λ) is generally set to 65% when the photon energy is equal to or greater than the gap energy. $S(\lambda)$ represents the number of photons in the AM 1.5 spectrum.

Table 9. The calculated open-circuit voltage V_{OC} (V), voltage loss V_{LOSS} (V), short-circuit density J_{SC} (mA/cm^2) and other parameters (eV) of all complexes.

D/A interface	E_g	H_D–L_A	L_D–L_A	V_{OC}	V_{LOSS}	J_{SC}
Ce_6Me_3/$PC_{71}BM$	2.21	2.09	0.39	1.79	0.42	14.10
Ce_6Me_3/DTBCIC-H	2.24	1.81	0.67	1.31	0.93	29.52
Ce_6Me_3/DTBCIC-F	2.22	1.74	0.74	1.24	0.98	30.14
Ce_6Me_3/DTBCIC-Cl	2.16	1.68	0.80	1.18	0.98	31.04

Table 9 shows the simulation values for these parameters. The H_D–L_A, closely related to V_{OC}, have the following order: Ce_6Me_3/$PC_{71}BM$ > Ce_6Me_3/DTBCIC-H > Ce_6Me_3/DTBCIC-F > Ce_6Me_3/DTBCIC-Cl. Therefore, the V_{OC} values have the same trend as H_D–L_A and are calculated to be 1.79 V, 1.31 V, 1.24 V and 1.18 V, respectively. The V_{LOSS} of the four investigated complexes were 0.42 V, 0.93 V, 0.98 V and 0.98 V, respectively. However, the energy difference of the LUMO L_D–L_A follows the reverse order to the values of H_D–L_A. It seems that Ce_6Me_3/$PC_{71}BM$ has a greater voltage but lower driving force for exciton separation. The J_{SC} values are calculated in the following order: Ce_6Me_3/$PC_{71}BM$ (14.10 mA·cm^{-2}) < Ce_6Me_3/DTBCIC-H (29.52 mA·cm^{-2}) < Ce_6Me_3/DTBCIC-F (30.14 mA·cm^{-2}) < Ce_6Me_3/DTBCIC-Cl (31.04 mA·cm^{-2}). It can be easily found that an OSC based on the Ce_6Me_3/DTBCIC-Cl heterojunction will have a higher photocurrent than that of other compound heterojunctions, nearly twice as much as Ce_6Me_3/$PC_{71}BM$. This is due to its excellent light absorption properties and higher charge mobility, suggesting that an OSC with halogenated NFA and a chlorophyll derivative may be a significant potential candidate for heterojunctions solar cells.

4. Conclusion

In this work we have compared the basic properties of the donor chlorophyll *a* derivative Ce_6Me_3, the fullerene acceptor $PC_{71}BM$ and the DTBCIC series of NFAs, including the structure, light absorption, electrochemical and photoelectric parameters. We found that Ce_6Me_3 and these investigated acceptors have suitable FMOs for combining into heterojunction OSCs. Chlorinated DTBCIC-Cl has excellent optoelectronic performance, such as better planarity, lower energy gap and recombination energy, larger EA and electrophilic index and relative redshift of the absorption spectrum. We then constructed four D/A interfacial models (experimental Ce_6Me_3/$PC_{71}BM$, and designed Ce_6Me_3/DTBCIC-H, Ce_6Me_3/ DTBCIC-F and Ce_6Me_3/DTBCIC-Cl) to further study the photovoltaic characteristics of chlorophyll-based OSCs. It is noteworthy that the Ce_6Me_3/DTBCIC-Cl interface has a higher K_{CS}/K_{CR}, suggesting its stronger charge transfer capability. The Ce_6Me_3/DTBCIC-Cl system has a stronger D/A interaction that is beneficial for promoting exciton dissociation and charge transfer. Next, we observed in the donor Ce_6Me_3 and NFA dimeric structures that the halogenated DTBCIC series molecules have better electron mobility, and the mobility effect after chlorination is more significant. Finally, the photovoltaic performance was also simulated, showing that although Ce_6Me_3/$PC_{71}BM$ has a slightly higher V_{OC}, its J_{SC} is much lower than that of NFAs. The higher J_{SC} exhibited by Ce_6Me_3/DTBCIC-Cl is mainly due to its favorable light absorption properties and charge mobility. It can be inferred that Ce_6Me_3/DTBCIC-Cl is a potential D/A interface candidate, and our work provides a pathway for designing high-performance chlorophyll-based OSCs.

Acknowledgements

We are very grateful to Shuoqi Sun for help and discussions regarding this study.

Project supported by the National Natural Science Foundation of China (Grant Nos. 12074059, 11974152, and 11404055) and Heilongjiang Postdoctoral Fund (Grant No. LBH-Q21061).

References

[1] He C L, Chen Z, Wang T H, Shen Z Q, Li Y K, Zhou J D, Yu J W, Fang H Y, Li Y H, Li S X, Lu X H, Ma W, Gao F, Xie Z Q, Coropceanu V, Zhu H M, Bredas J L, Zuo L J and Chen H Z 2022 *Nat. Commun.* **13** 2598

[2] Guo Y, Han G C and Yi Y P 2022 *Angew. Chem. Int. Ed.* e202205975

[3] Li T F and Zhan X W 2021 *Acta Chim. Sin.* **79** 257

[4] Che Y X, Niazi M R, Izquierdo R and Dmitrii F P 2021 *Angew. Chem. Int. Ed.* **60** 24833

[5] Wang J Y and Zhan X W 2021 *Acc. Chem. Res.* **54** 132

[6] Bifari E N, Almeida P and El-Shishtawy R M 2023 *Mater. Today Energy* **36** 101337

[7] He C L, Pan Y W, Wu B H, Xia X X, Chen Z, Zhu H M, Ma C Q, Lu X H, Ma W, Lu G H, Zuo L J and Chen H Z 2022 *Adv. Mater.* 202203379

[8] Mahmood A and Wang J L 2021 *Energy Environ. Sci.* **14** 90

[9] Piradi V, Yan F, Zhu X J and Wong W Y 2021 *Mater. Chem. Front.* **5** 7119

[10] Liu X J, Shao Y Y, Lu T, Chang D P, Li M J and Lu W C 2022 *Mater. Des.* **216** 110561

[11] Zhang Q, Zheng Y J, Sun W B, Ou Z P, Odunmbaku O, Li M, Chen S S, Zhou Y L, Li J, Qin B and Sun K 2022 *Adv. Sci.* **9** 2104742

[12] Yang J, Li Q S and Li Z S 2021 *Phys. Chem. Chem. Phys.* **23** 12321

[13] Greenstein B L and Hutchison G R 2022 *J. Phys. Chem. Lett.* **13** 4235

[14] Zhao C C, Wang J X, Zhao X Y, Du Z L, Yang R Q and Tang J G 2021 *Nanoscale* **13** 2181

[15] Yu G, Gao J and Hummelen J C 1995 *Science* **270** 1789

[16] Alem S, de Bettignies R, Nunzi J M and Cariou M 2004 *Appl. Phys. Lett.* **84** 2178

[17] Nguyen L H, Hoppe H, Erb T, Gunes S, Gobsch G and Sariciftci N S 2007 *Adv. Funct. Mater.* **17** 1071

[18] Wang Y W, Wang X F, Zhang J P, Hong Z, Kido J, Kitao O, Ikeuchi T, Tamiaki H and Sasaki S 2012 *J. Phys. Chem. C* **116** 21244

[19] Duan S N, Zhou Q, Dall'Agnese C X, Chen G, Wang X F, Tamiaki H, Sakai K, Ikeuchi T and Sasaki S 2019 *Sol. RRL* **3** 1900203

[20] Duan S N, Zhou Q, Li AJ, Wang X F, Sasaki S and Tamiaki H 2020 *Sol. RRL* **4** 2000162

[21] Duan S N, Song J X, Zhou E J, Yang K, Lu S R, Li D F, Sasaki S, Tamiaki H and Wang X F 2022 *J. Phys. Chem. C* **126** 4807

[22] Yan C Q, Barlow S, Wang Z H, Yan H, Jen A K Y, Marder S R and Zhan X W 2018 *Nat. Rev. Mater.* **3** 18003

[23] Ye L, Hu H W, Ghasemi M, Wang T H, Collins B A, Kim J H, Jiang K, Carpenter J H, Li H, Li Z K, McAfee T, Zhao J B, Chen X K, Lai J L Y, Ma T X, Bredas J L, Yan H and Ade H 2018 *Nat. Mater.* **17** 253

[24] Liu W, Xu X, Yuan J, Leclerc M, Zou Y P and Li Y F 2021 *ACS Energy Lett.* **6** 598

[25] Privado M, de la Cruz P, Malhotra P, Sharma G D and Langa F 2021 *Sol. Energy* **221** 393

[26] UrRehman S, Anwer M, BiBi S, Jamil S, Yasin M, Khan S R, Nadeem R, Ali S and Jia R 2022 *Mater. Sci. Semicond. Process.* **140** 106381

[27] Shao Y Y, Lu T, Li M J and Lu W C 2022 *New J. Chem.* **46** 3370

[28] Ahmed S and Kalita D J 2020 *Phys. Chem. Chem. Phys.* **22** 23586

[29] Gao W, Liu T, Ming R J, Luo Z H, Wu K L, Zhang L, Xin J M, Xie D J, Zhang G Y, Ma W, Yan H and Yang C L 2018 *Adv. Funct. Mater.* **28** 1803128

[30] Ma X L, Wang J, Gao J H, Hu Z H, Xu C Y, Zhang X L and Zhang F J 2020 *Adv. Energy Mater.* **10** 2001404

[31] Guo X, Fan Q P, Wu J N, Li G W, Peng Z X, Su W Y, Lin J, Hou L T, Qin Y P, Ade H, Ye L, Zhang M J and Li Y F 2021 *Angew. Chem. Int. Ed.* **60** 2322

[32] Yu H, Qi Z Y, Zhang J Q, Wang Z, Sun R, Chang Y, Sun H L, Zhou W T, Min J, Ade H and Yan H 2020 *J. Mater. Chem. A* **8** 23756

[33] Geng S Z, Yang W T, Gao J, Li S X, Shi M M, Lau T K, Lu X H, Li C Z and Chen H Z 2019 *Chin. J. Polym. Sci.* **37** 1005

[34] Liu X Z, Wei Y N, Zhang X, Qin L Q, Wei Z X and Huang H 2021 *Sci. China Chem.* **64** 228

[35] Wang S H, Duan S N, Wang Y W, Sun C L, Wang X F and Sasaki S 2019 *J. Energy Chem.* **38** 88

[36] Tang Y X, Feng H X, Liang Y Y, Tang H R, Du Z R, Xu J X, Huang F and Cao Y 2021 *ACS Appl. Polym. Mater.* **5** 2298

[37] Efrem A, Lim C J, Lu Y and Ng S C 2014 *Tetrahedron Lett.* **55** 4849

[38] Li S X, Zhan L L, Zhao W C, Zhang S H, Ali B, Fu Z S, Lau T K, Lu X H, Shi M M, Li C Z, Hou J H and Chen H Z 2018 *J. Mater. Chem. A* **6** 12132

[39] Hohenberg P and Kohn W 1964 *Phys. Rev.* **136** B864

[40] Kohn W and Sham L 1965 *Phys. Rev.* **137** A1697

[41] Becke A D 1988 *Phys. Rev. A* **38** 3098

[42] Lee C, Yang W and Parr R G 1988 *Phys. Rev. B* **37** 785

[43] Grimme S, Ehrlich S and Goerigk L 2011 *J. Comput. Chem.* **32** 1456

[44] Mu X J, Wang X X, Quan J and Sun M T 2020 *J. Phys. Chem. C* **124** 4968

[45] Schweda B, Reinfelds M, Hofinger J, Baumel G, Rath T, Kaschnitz P, Fischer R C, Flock M, Amenitsch H, Scharber M C and Trimmel G 2022 *Chem. Eur. J.* **28** e202200276

[46] Sun B Y, Ren X, Li J and Chen J N 2023 *J. Phys. Chem. C* **127** 15346

[47] Gross E K U and Kohn W 1985 *Phys. Rev. Lett.* **55** 2850

[48] Yanai T, Tew D P and Handy N C 2004 *Chem. Phys. Lett.* **393** 51

[49] Mattsson A E, Armiento R, Schultz P A and Mattsson T R 2006 *Phys. Rev. B* **73** 195123

[50] Niu Y L, Li W Q, Peng Q, Geng H, Yi Y P, Wang LJ, Nan G J, Wang D and Shuai Z G 2018 *Mol. Phys.* **116** 1078

[51] Nan G J, Yang X D, Wang L J, Shuai Z G and Zhao Y 2009 *Phys. Rev. B* **79** 115203

[52] Shuai Z G, Geng H, Xu W, Liao Y and André J M 2014 *Chem. Soc. Rev.* **43** 2662

[53] Shuai Z G, Wang D, Peng Q and Geng H 2014 *Acc. Chem. Res.* **47** 3301

[54] Liu Z Y, Lu T and Chen Q X 2020 *Carbon* **165** 468

[55] Li B, Cao B F, Zhou Q, Li Y, Bao Y J, Shi Y, Liu C L, Jin M X, Gao J B and Ding D J 2021 *J. Mater. Chem. C* **9** 14388

[56] Frisch M J, Trucks G W, Schlegel H B, *et al.* 2009 *Gaussian 09 Revision B01*

[57] Lu T and Chen F W 2012 *J. Comput. Chem.* **33** 580

[58] Lu T and Chen F W 2012 *J. Mol. Graph. Model* **38** 314

[59] Pomogaeva A V, Scheer M and Timoshkin A Y 2018 *Chem. Eur. J.* **24** 17046

[60] Zang Z F, Yu Y, Song P, Ma F C and Li Y Z 2023 *J. Phys. Chem. C* **127** 110

[61] Zhang J and Lu T 2021 *Phys. Chem. Chem. Phys.* **23** 20323

[62] Sirohi A, SanthiBhushan B and Srivastava A 2021 *J. Mol. Model.* **27** 77

[63] Alexandre R A F, de Oliveira O V and dos Santos J D 2021 *Chem. Phys. Lett.* **766** 138328

[64] Gai X W, Sheng H and Wang J A 2023 *Phys. Chem. Chem. Phys.* **25** 20049

[65] Zhang K Y, Wei Z Q, Song P, Ma F C and Li Y Z 2022 *Sol. Energy* **248** 160

[66] Nebbach D, Agda F, Kaya S, Siddique F, Lakhlifi T, Ajana M A and Bouachrine M 2022 *J. Mol. Liq.* **348** 118289

[67] Aboulouard A, Mtougui S, Demir N, Moubarik A, El Idrissi M and Can M 2021 *Synth. Met.* **279** 116846

[68] Zhou B, Hu Z, Jiang Y, He X, Sun Z and Sun H 2018 *J. Phys.: Condens. Matter* **30** 215501

[69] Sun W, Bu Y and Wang Y 2014 *Design and Applications of Nanomaterials for Sensors* **16** 31

[70] Lee J C, Chai J D and Lin S T 2015 *RSC Adv.* **5** 101370

[71] Chattaraj P K, Sarkar U and Roy D R 2006 *Chem. Rev.* **106** 2065

[72] Marcus and Rudolph 1993 *Rev. Mod. Phys.* **65** 599

[73] Calvo-Castro J, Mchugh C J and Mclean A J 2015 *Dyes Pigm.* **113** 609

[74] Imahori H, Yamada H, Guldi D M, Shimomura A, Kundu S, Yamada K, Sakata Y and Fukuzumi S 2002 *Angew. Chem. Int. Ed.* **41** 2344

[75] Koese M E, Mitchell W J, Kopidakis N, Chang C H, Shaheen S E, Kim K and Rumbles G 2007 *J. Am. Chem. Soc.* **129** 14257

[76] Wang Q G, Zeng Z Y, Li Y Z and Chen X R 2020 *Sol. Energy* **208** 10

[77] Li Y, Sasaki S, Tamiaki H, Liu C L, Song J X, Tian W J, Zheng E Q, Wei Y J, Chen G, Fu X Q and Wang X F 2015 *J. Power Sources* **297** 519

[78] Han C Y, Wang J X, Chen L L, Chen J F, Zhou L, Wang P C, Shen W F, Zheng N, Wen S G, Li Y H and Bao X C 2021 *Adv. Funct. Mater.* **31** 2107026

[79] Cui Y J, Zhu P P, Shi X L, Liao X F and Chen Y W 2021 *J. Phys. Chem. C* **125** 10250

[80] Xu Y, Yao H F, Ma L J, Hong L, Li J Y, Liao Q, Zu Y F, Wang J W, Gao M Y, Ye L and Hou J H 2020 *Angew. Chem. Int. Ed.* **59** 9004

[81] Shao Y Y, Lu T, Li M J and Lu W C 2022 *New J. Chem.* **46** 3370

[82] Emelianova E V, van der Auweraer M and Bässler H 2008 *J. Chem. Phys.* **128** 224709

[83] Zhen C G, Becker U and Kieffer J 2009 *J. Phys. Chem. A* **113** 9707

[84] Kraner S, Prampolini G and Cuniberti G 2017 *J. Phys. Chem. C* **121** 17088

[85] Haroon M, Akhtar T, Khalid M, Mehmood H, Asghar M A, Baby R, Orfali R and Perveen S 2013 *RSC Adv.* **13** 7237

[86] Zang Z F, Wang Q G, Song P, Ma F C and Li Y Z 2022 *Sol. Energy* **231** 503

[87] Xiang C C, Zhao Q M, Liu W Q, Cao J M, Zou Y P and Zhou H 2022 *J. Mater. Chem. A* **10** 25611

[88] Cave RJ and Newton MD 1996 *Chem. Phys. Lett.* **249** 15

[89] Cossi M, Rega N, Scalmani G and Barone V 2003 *J. Comput. Chem.* **24** 669

[90] Biswas S, Pramanik A, Pal S and Sarkar P 2017 *J. Phys. Chem. C* **121** 2574

[91] Lemaur V, Steel M, Beljonne D, Bredas J L and Cornil J 2005 *J. Am. Chem. Soc* **127** 6077

[92] Kose M E and Schanze K S 2020 *J. Phys. Chem. A* **124** 9478

[93] Zhao H F, Yin H, Liu X C, Li H, Shi Y, Liu C L, Jin M X, Gao J B, Luo Y and Ding D J 2019 *J. Phys. Chem. Lett.* **10** 3064

[94] Shen F G, Peng A D, Chen Y, Dong Y, Jiang Z W, Wang Y B, Fu H B and Yao J N 2008 *J. Phys. Chem. A* **112** 2206

[95] Christians J A, Fung R C M and Kamat P V 2014 *J. Am. Chem. Soc.* **136** 758

[96] Irfan A, Assiri M and Al-Sehemi AGJOE 2018 *Org. Electron.* **57** 211

[97] Zhang W, Hu R, Zeng X K, Su X J, Chen Z F, Zou X S, Peng J, Zhang C Y and Yartsev A 2019 *Polymers* **11** 408

[98] Zhu R, Li Q S and Li Z S 2019 *J. Mater. Chem. A* **7** 16304

[99] Scharber M C, Mühlbacher D, Koppe M, Denk P, Waldauf C, Heeger A J and Brabec C L 2006 *Adv. Mater.* **18** 789

[100] Street R A, Hawks S A, Khlyabich P P, Li G, Schwartz B J, Thompson B C and Yang Y 2014 *J. Phys. Chem. C* **118** 21873

[101] Bijleveld J C, Verstrijden R A M, Wienk M M and Janssen R A J 2010 *Appl. Phys. Lett.* **97** 073304

[102] Wu L N, Yin H, Li M Y, Sun G Y and Jin G D 2019 *Comput. Theor. Chem.* **1156** 37

[103] Lu Q C, Wang Q G, Song P, Ma F C, Yang Y H and Li Y Z 2021 *Sol. RRL* **5** 2100670